# Experimental study of a stiff wave barrier in gelatine

Pieter Coulier[a,*], Hugh E.M. Hunt[b]

[a] *KU Leuven, Department of Civil Engineering, Kasteelpark Arenberg 40, B-3001 Leuven, Belgium*
[b] *University of Cambridge, Department of Engineering, Trumpington Street, Cambridge CB2 1PZ, United Kingdom*

**Abstract**

Railway induced vibrations and re–radiated noise in buildings can be mitigated by means of wave barriers in the soil. Numerical simulations demonstrate that a stiff wave barrier, consisting of a material that is stiffer than the surrounding medium, can be very effective if the stiffness contrast between the barrier and the medium is sufficiently large. This technical note presents results of a lab experiment that has been carried out to validate these findings, using gelatine instead of soil in order to reduce the wavelengths and thus the scale of the test setup. An expanded polystyrene beam is employed as wave barrier, while a non–contact measurement procedure is applied for visualizing the waves in the gelatine, based on reflections of a grid of laser rays. The experimental results are found to be in line with the numerical predictions, confirming the vibration reduction effectiveness of stiff wave barriers.

*Keywords:* Dynamic soil–structure interaction, elastodynamic wave propagation, wave barrier, lab experiment, non–contact measurement procedure.

## 1. Introduction

Railway induced vibrations are an important source of annoyance in the built environment. These vibrations are generated at the wheel–rail interface, propagate as elastic waves in the soil and excite surrounding buildings, where they cause disturbance of sensitive equipment and discomfort to people ($1-80\,\mathrm{Hz}$), while re–radiated noise ($16-250\,\mathrm{Hz}$) may be perceived when eigenmodes of floors and walls are excited. Various measures can be taken to mitigate vibrations, either at the source (railway track) [1], on the propagation path between source and receiver (soil) [2], or at the receiver (buildings) [3]. An advantage of interventions on the propagation path is that no modifications of the track are required, while multiple buildings can be shielded simultaneously from vibration. Furthermore, this type of measures can relatively easily be implemented in existing situations. Typical examples are vibration isolation screens [4, 5, 6], buried wall barriers [7, 8], and wave impeding blocks [9].

The vibration reduction efficiency of a stiff wave barrier (i.e. consisting of a material that is stiffer than the original soil) has recently been investigated in detail in [10]. It has been demonstrated that its effectiveness depends on the stiffness contrast between the barrier and the soil; the larger the contrast, the more effective the barrier is. Furthermore, it is found that a reduction of vibration levels can only be achieved above a certain critical frequency and in a limited area behind the barrier.

It is crucial to validate the outcome of the numerical simulations by means of experiments. A field experiment has been designed and carried out within the frame of the EU FP7 project RIVAS [11], using overlapping jet grout columns for the construction of a stiff wave barrier of $1\,\mathrm{m} \times 7.5\,\mathrm{m} \times 55\,\mathrm{m}$ along a railway track in Spain. Although such field tests are very valuable, it is often very difficult to control all parameters (e.g. soil conditions, barrier geometry, source of excitation, etcetera) which leads to many sources of uncertainty when processing the experimental data. It is therefore worthwhile to complement these (rather expensive) in situ experiments with small scale lab experiments under more manageable conditions.

*Corresponding author. Phone: + 32 16 32 23 78. Fax: + 32 16 32 19 88.
*Email address:* pieter.coulier@bwk.kuleuven.be (Pieter Coulier)

*Postprint published in Soil Dynamics and Earthquake Engineering*

This technical note reports on a low–cost experimental study that has been performed to investigate the effectiveness of stiff wave barriers, using gelatine instead of soil. The text is organized as follows. First, the physical mechanism that leads to a reduction of vibration levels is summarized. Next, the experimental setup is discussed; special attention is paid to a non–contact measurement procedure. Finally, the experimental results are discussed and compared to the numerical predictions.

## 2. Physical mechanism

The vibration reduction efficiency of stiff wave barriers has been investigated in detail in [10] and [12] by means of a coupled finite element – boundary element approach, taking the semi–infinite extent of the soil into account. The physical mechanism is briefly discussed in the following for a case study of a barrier in a homogeneous halfspace.

The halfspace is characterized by a shear wave velocity $C_\mathrm{s} = 200\,\mathrm{m/s}$, a dilatational wave velocity $C_\mathrm{p} = 400\,\mathrm{m/s}$, a density $\rho = 2000\,\mathrm{kg/m^3}$, and hysteretic material damping ratios $\beta_\mathrm{s} = \beta_\mathrm{p} = 0.025$ in deviatoric and volumetric deformation. Figure 1a shows the real part of the vertical displacement $\hat{u}_z(\mathbf{x},\omega)$ in the soil due to a harmonic point load at 30 Hz at the surface of the halfspace. The propagation of Rayleigh waves with a wavelength $\lambda_\mathrm{R}(f) = 6.2\,\mathrm{m}$ can clearly be observed. Figure 1b shows the wavefield in the soil in case a barrier of $2\,\mathrm{m} \times 2\,\mathrm{m}$ is included in the halfspace. The barrier is assumed to be of infinite length and consists of a material with a shear wave velocity $C_\mathrm{s} = 550\,\mathrm{m/s}$, a dilatational wave velocity $C_\mathrm{p} = 950\,\mathrm{m/s}$, and the same the density and material damping ratios as those in the halfspace. Almost no reduction of vibration levels is achieved in a sharply delimited central area behind the barrier, while a much stronger reduction is observed outside this area. The vibration reduction efficiency is quantified in figure 1c through the vertical insertion loss $\widehat{\mathrm{IL}}_z(\mathbf{x},\omega)$:

$$\widehat{\mathrm{IL}}_z(\mathbf{x},\omega) = 20\log_{10}\frac{|\hat{u}_z^\mathrm{ref}(\mathbf{x},\omega)|}{|\hat{u}_z(\mathbf{x},\omega)|} \tag{1}$$

which compares the vertical displacement $\hat{u}_z^\mathrm{ref}(\mathbf{x},\omega)$ in the reference case (without a barrier) to the vertical displacement $\hat{u}_z(\mathbf{x},\omega)$ in case a barrier is included. Positive values of the insertion loss indicate a reduction of the vertical free field vibrations. Figure 1c shows that the insertion loss reaches up to 10 dB, corresponding to a reduction of vibration levels by a factor of three.

As discussed in [10, 12], the peculiar pattern observed in figure 1c is due to the interaction between Rayleigh waves in the soil and bending waves in the stiff wave barrier. The propagation of plane waves in the soil with a trace wavelength smaller than the barrier's bending wavelength is impeded due to the latter's bending stiffness. This only occurs above a critical frequency $f_\mathrm{c}$ at which the Rayleigh wavelength in the soil matches the free bending wavelength in the barrier [10]:

$$f_\mathrm{c} = \frac{C_\mathrm{R}^2}{2\pi}\sqrt{\frac{\rho A}{EI}} \tag{2}$$

where $C_\mathrm{R}$ is the Rayleigh wave velocity in the soil, while $E$ is the Young's modulus, $\rho$ the density, $A$ the cross sectional area, and $I$ the area moment of inertia of the barrier. The critical frequency equals 12 Hz in the present case, explaining why the barrier is effective at 30 Hz as seen in figure 1c. A critical angle $\theta_\mathrm{c}(f)$ delimiting an area where vibration levels are reduced can be defined as well, determined by the ratio of the Rayleigh wavelength in the soil and the free bending wavelength in the barrier [10]:

$$\theta_\mathrm{c}(f) = \sin^{-1}\left(\frac{C_\mathrm{R}}{\sqrt{2\pi f}}\left(\frac{\rho A}{EI}\right)^{1/4}\right) \tag{3}$$

This angle can clearly be distinguished in figure 1c.

The physical mechanism outlined above closely resembles the phenomenon of coincidence in acoustics [13], where sound waves impinging on an infinite plate are freely transmitted if the wavelength of bending waves

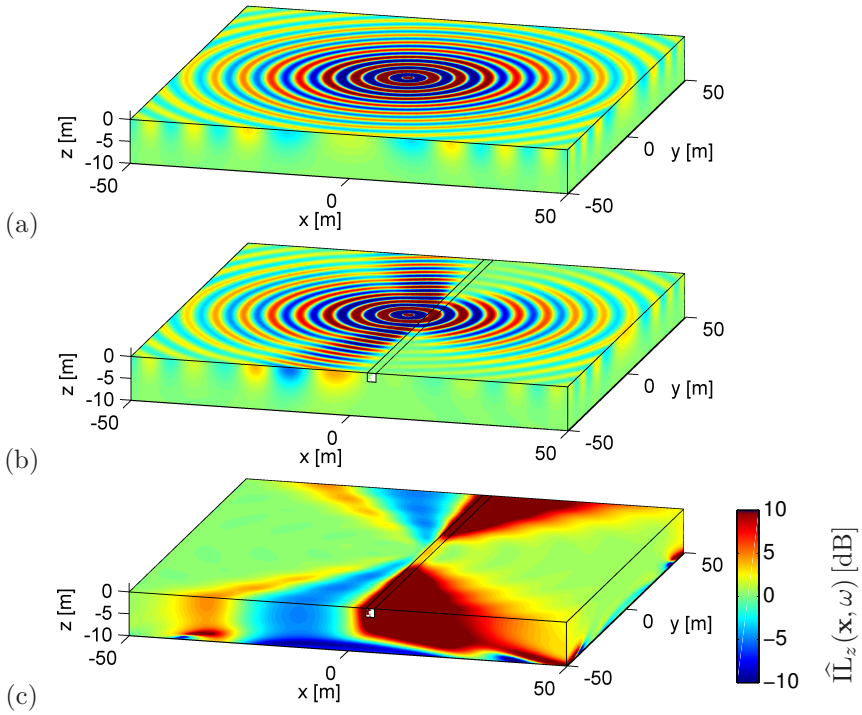


Figure 1: Real part of the vertical displacement $\hat{u}_z(\mathbf{x},\omega)$ at 30 Hz (a) without and (b) with a stiff wave barrier. The corresponding insertion loss $\widehat{\mathrm{IL}}_z(\mathbf{x},\omega)$ is shown in (c).

in the plate equals the trace wavelength of the acoustic waves in the air. In acoustics, the transmission loss below coincidence is predominantly related to the so–called mass law [13]. At the coincidence frequency, a prominent dip occurs in the transmission loss, while it increases significantly at higher frequencies due to the plate's bending stiffness. In the present case, a reduction of vibration levels is only seen above coincidence, attributed to the barrier's bending stiffness, while the inertia effect is negligible.

## 3. Experimental setup

As mentioned in the introduction, the aim is to demonstrate the existence of the theoretically predicted critical frequency $f_\mathrm{c}$ and critical angle $\theta_\mathrm{c}(f)$ (equations (2) and (3)) by means of a simple lab experiment. Typical values for the Rayleigh wave velocity $C_\mathrm{R}$ in the soil range from as low as 50 m/s (e.g. for peat) up to 800 m/s or higher (e.g. for rock materials) [14]. Within the frequency range of interest, the Rayleigh wavelength $\lambda_\mathrm{R}(f) = C_\mathrm{R}/f$ is thus of the order of (tens of) meters, making it infeasible to use actual soil deposits in a small scale experiment. The search for an alternative elastic solid with appropriate dynamic characteristics led to a rather uncommon material, i.e. gelatine.

The experimental setup is shown in figure 2. A test sample was created by pouring a mixture of gelatine crystals and boiling water into a plexiglass tank of 0.90 m × 0.85 m × 0.10 m. The gelatine subsequently solidified in a refrigerated room at an average temperature of 3° C. An expanded polystyrene beam served as stiff wave barrier. In order to avoid damage to the gelatine, this beam was not embedded in the gelatine but positioned on top of its surface; numerical simulations have demonstrated that the barrier is in that case also effective. A shaker was used for applying a vertical harmonic excitation on the gelatine's surface. The presence of boundaries in the test setup is not in correspondence with the unbounded nature of the soil. Wave reflections inevitably take place at the boundaries of the plexiglass tank, which might disturb the experimental results. The wavelengths in the gelatine remain relatively small compared to the dimensions of the tank, however, and it is therefore believed that such reflections are only of minor importance.

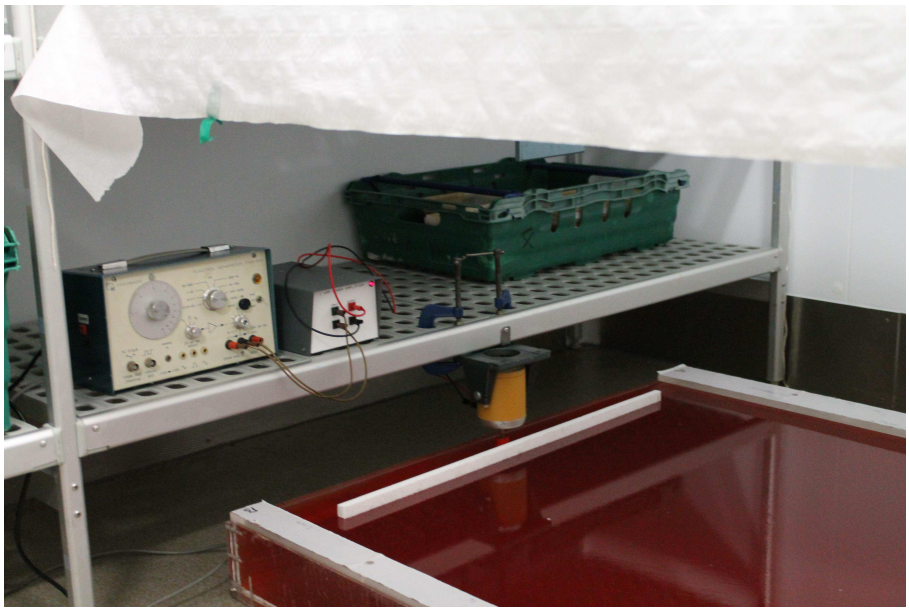

Figure 2: The experimental setup, consisting of a plexiglass tank filled with gelatine, an expanded polystyrene beam, and a harmonic shaker.

The mechanical properties of a low stiffness material as gelatine are not easily determined by classical mechanical tests, but can be obtained through innovative techniques such as nano–indentation tests [15, 16, 17]. No such tests could be performed on the actual gelatine sample, however. Based on results reported in the literature [15, 17], the gelatine is assumed to have a density $\rho = 1000\,\mathrm{kg/m^3}$, a shear modulus $\mu = 10\,\mathrm{kPa}$ and a bulk modulus $K = 2.2\,\mathrm{GPa}$, leading to a Rayleigh wave velocity $C_\mathrm{R} = 3\,\mathrm{m/s}$. Gelatine is a quasi–incompressible medium, as opposed to (unsaturated) soils that usually have a Poisson's ratio of about 0.3. Numerical simulations have demonstrated, however, that a stiff wave barrier is also effective if embedded in a medium with a Poisson's ratio close to 0.5, suggesting that gelatine is suited for this experiment. The barrier in the test setup has a square cross section $A = 0.015\,\mathrm{m} \times 0.015\,\mathrm{m}$ and consists of expanded polystyrene foam with a density $\rho = 75\,\mathrm{kg/m^3}$ and an estimated Young's modulus $E = 500\,\mathrm{kPa}$. Evaluating equation (2) with the foregoing set of parameters results in a critical frequency $f_\mathrm{c} = 4.3\,\mathrm{Hz}$.

Visualizing and measuring the wavefield in the gelatine turned out to be a challenging task, as the gelatine's fragility made it infeasible to attach sensors to its surface. A non–contact measurement technique was thus required, taking into account practical constraints such as the fact that all measurements had to take place inside the refrigerated room and that the experiment should remain inexpensive. The procedure that has been applied is illustrated in figure 3. A laser pointer is used to project a regular grid of laser rays on the gelatine's surface, which are reflected and then visualized on a sheet of thin, translucent paper suspended above the gelatine. These reflections are subsequently photographed using an exposure time of 60 s, ensuring that a sufficient amount of light reaches the image sensor of the camera. While the reflected laser rays remain very focused if the gelatine is not excited (figure 4), the reflections are dispersed if waves are propagating in the gelatine, resulting in a blurred image (figure 5). The extent to which the laser rays are dispersed hence gives an indication of the vibration amplitude at each point, enabling a quantification of the wavefield.

## 4. Results and discussion

Figure 4a shows the reflected laser grid in case no excitation is applied to the gelatine. As the gelatine's surface is not vibrating, the emitted laser rays are almost not dispersed, which leads to focused reflections.

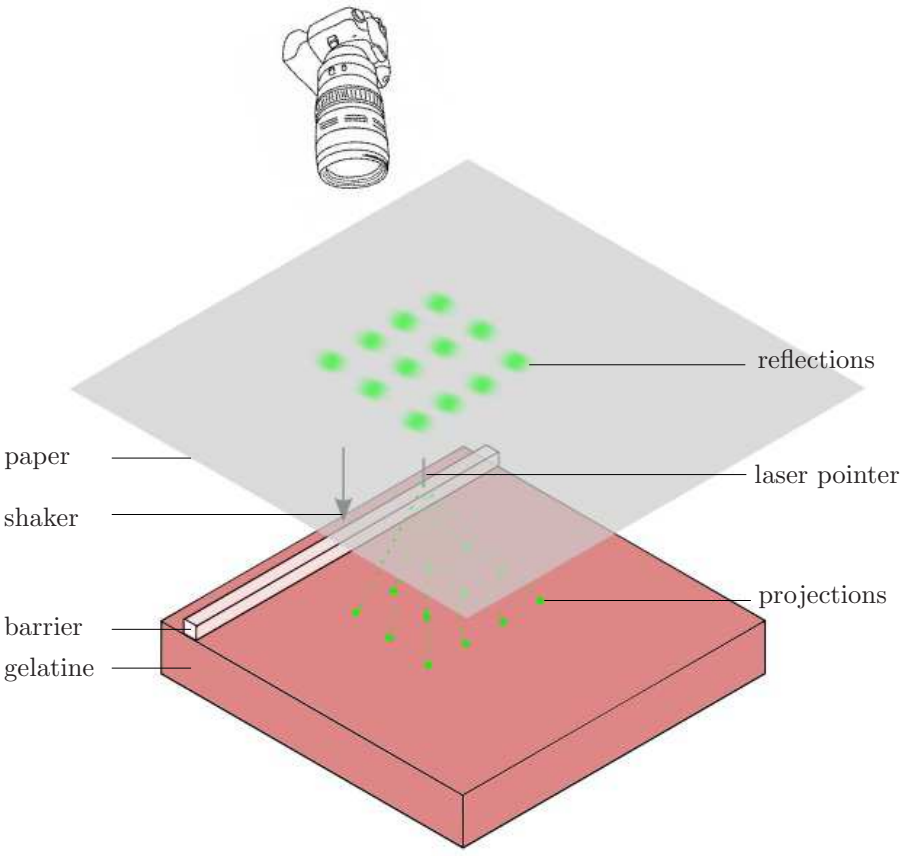


Figure 3: Schematic overview of the experimental setup and the non–contact measurement procedure.

The Image Processing Toolbox of MATLAB [18] is employed for processing this original image and for identifying the distinct reflections. The original truecolor image is first converted into a grayscale image and subsequently into a binary black/white image (using a threshold of 0.60 on the luminance level). Morphological opening and closing operations are then performed on this binary image in order to remove noisy spots (consisting of only a few pixels) and to fill small gaps of pixels within each area of clearly reflected laser rays, respectively. A Gaussian filter is finally applied in order to enhance the edge detection of the distinct laser reflections. The processed image is shown in figure 4b.

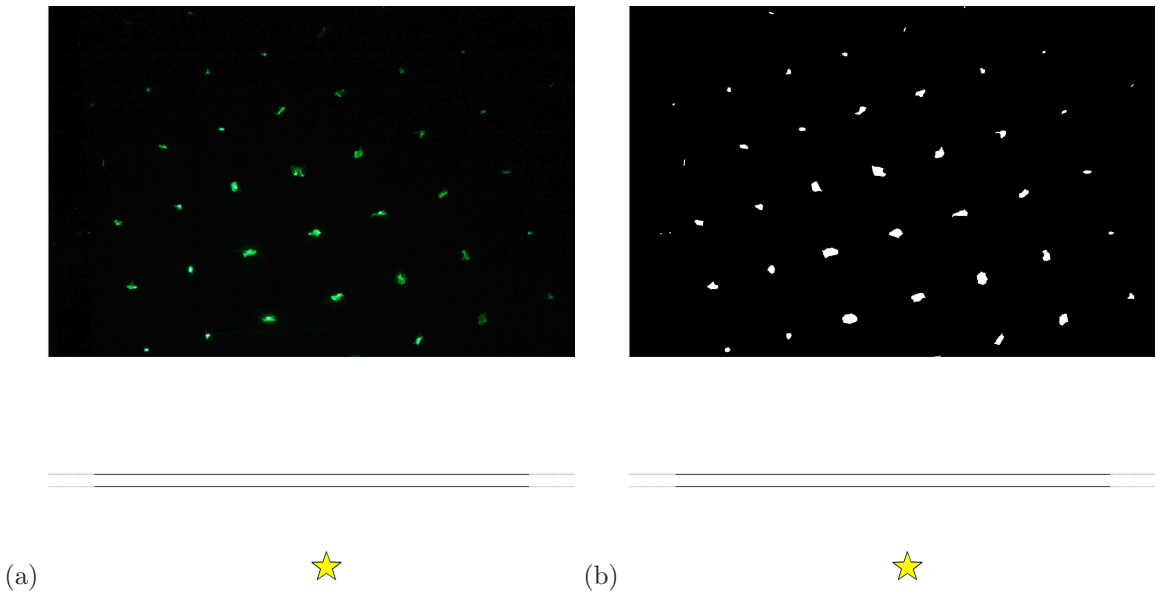


Figure 4: (a) Original image and (b) identified reflections in case no excitation is applied to the gelatine. The position of the shaker is indicated with a star.

Figure 5a shows the reflections in case of harmonic excitation at 15 Hz (i.e. above the critical frequency $f_c$); the postprocessed image is shown in figure 5b. These reflections are now elongated and aligned along the wave propagation direction (i.e. perpendicular on the wavefronts). Figure 6 shows an extrapolated contourplot of the number of pixels in the areas identified in figure 5b, hence providing an indication of the amplitude of the vibrations at each point. Superimposed are circular arcs that are concentric around the source of excitation. The amplitudes are large in the central area behind the barrier but are considerably reduced outside this area. This observation seems to confirm the existence of a critical angle, although it is not as apparent as in figure 1.

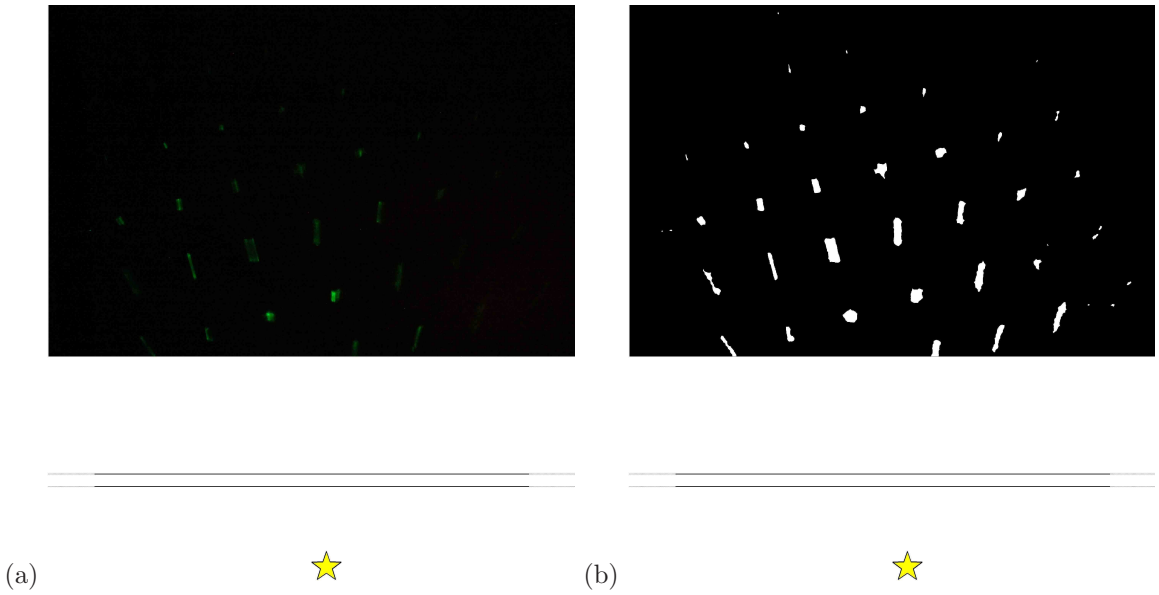


Figure 5: (a) Original image and (b) identified reflections in case of harmonic excitation at 15 Hz. The position of the shaker is indicated with a star.

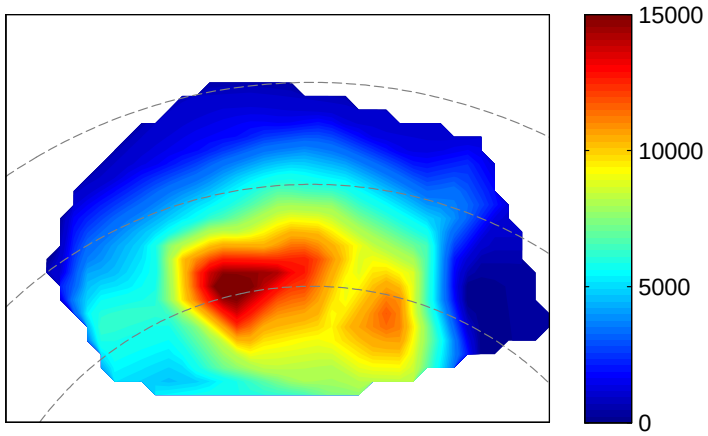


Figure 6: Contourplot of the area of the reflected laser rays in case of harmonic excitation at 15 Hz. The red colour corresponds to high vibration amplitudes.

Figure 7a shows the reflections in case of harmonic excitation at 30 Hz. The postprocessed image and the resulting contourplot are shown in figure 7b and 8, respectively; the same colourscale as in figure 6 is used for the latter. It can be seen that the reflections are almost not dispersed, indicating that the gelatine is hardly vibrating. This suggests that the barrier is very effective at this frequency, which is in line with the numerical simulations.

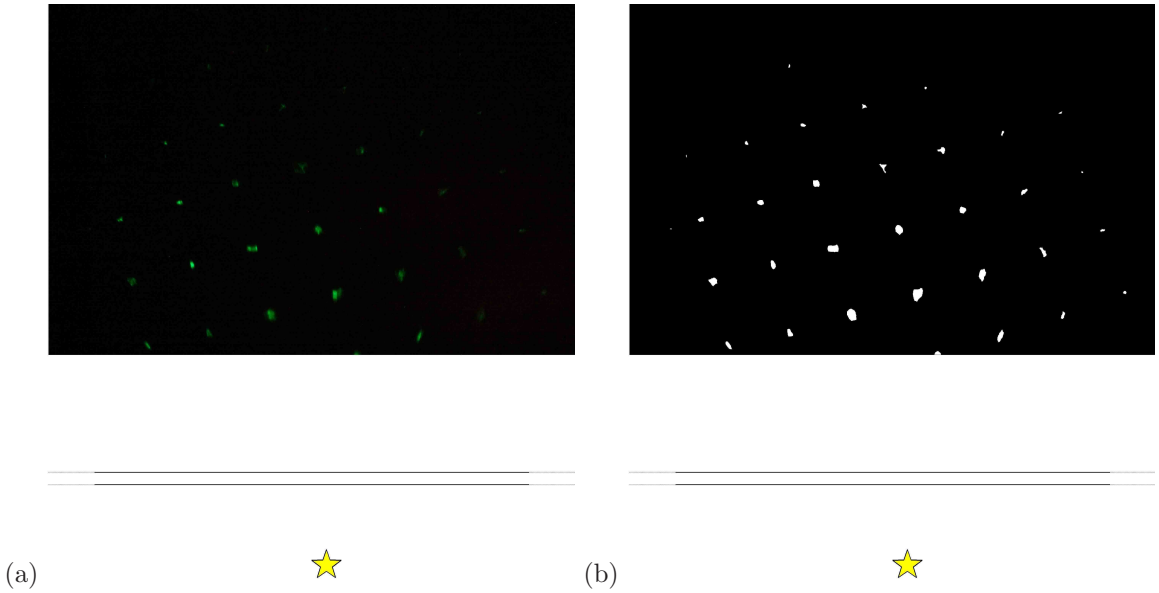


Figure 7: (a) Original image and (b) identified reflections in case of harmonic excitation at 30 Hz. The position of the shaker is indicated with a star.

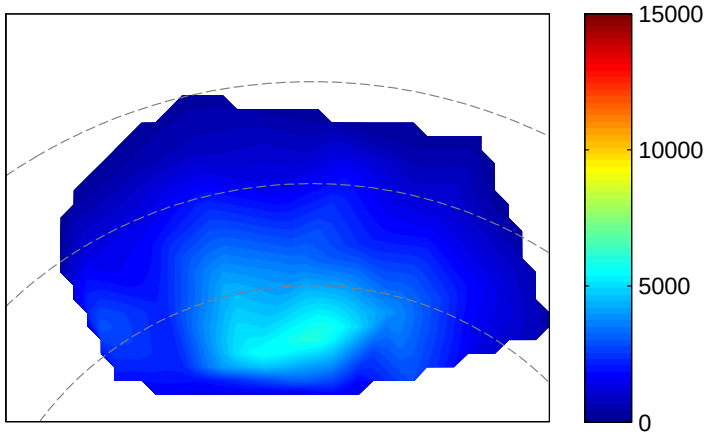


Figure 8: Contourplot of the area of the reflected laser rays in case of harmonic excitation at 30 Hz. The red colour corresponds to high vibration amplitudes.

## 5. Conclusion

In this technical note, the effectiveness of stiff wave barriers for impeding the propagation of Rayleigh waves has been discussed. This type of barrier can be constructed in the soil to mitigate vibrations originating from railway traffic. Numerical simulations indicate that the vibration reduction efficiency is determined by the interaction of Rayleigh waves in the medium and bending waves in the barrier; this leads to the existence of a critical frequency and a critical angle. A small scale experiment has been carried out to validate these findings, using gelatine instead of soil as elastic medium and an expanded polystyrene beam as barrier. A non–contact technique was employed for visualizing the wavefield in the gelatine. The experimental results seem to confirm the effectiveness of a stiff wave barrier, especially at high frequencies.


## Acknowledgements

The authors would like to thank Mr Ian Reinhardt (Trinity College Cambridge), Mr Gareth Ryder (University of Cambridge, Department of Engineering), and Mr Francesco Battocchio (University of Cambridge, Department of Engineering) for their assistance with the experiments, and Dr Alexandre Kabla (University of Cambridge, Department of Engineering) for estimating the mechanical properties of gelatine.

The first author is a doctoral fellow of the Research Foundation Flanders (FWO). This work was performed while the first author was a visiting researcher at the University of Cambridge, supported by a Travel Grant of FWO. The financial support is gratefully acknowledged.


## References


[1] G. Lombaert, G. Degrande, B. Vanhauwere, B. Vandeborght, S. François, The control of ground borne vibrations from railway traffic by means of continuous floating slabs, Journal of Sound and Vibration 297 (3-5) (2006) 946–961.

[2] C. With, M. Bahrekazemi, A. Bodare, Wave barrier of lime-cement columns against train-induced ground-borne vibrations, Soil Dynamics and Earthquake Engineering 29 (6) (2009) 1027–1033.

[3] J. Talbot, H. Hunt, Isolation of buildings from rail tunnel vibration: a review, Journal of Building Acoustics 10 (3) (2003) 177–192.

[4] R. Woods, Screening of surface waves in soils, Journal of the Soil Mechanics and Foundation Division, Proceedings of the ASCE 94 (SM4) (1968) 951–979.

[5] E. Celebi, S. Firat, G. Beyhan, I. Cankaya, I. Vural, O. Kirtel, Field experiments on wave propagation and vibration isolation by using wave barriers, Soil Dynamics and Earthquake Engineering 29 (5) (2009) 824–833.

[6] D. Connolly, A. Giannopoulos, W. Fan, P. Woodward, M. Forde, Optimising low acoustic impedance back-fill material wave barrier dimensions to shield structures from ground borne high speed rail vibrations, Construction and Building Materials 44 (2013) 557–564.

[7] L. Andersen, S. Nielsen, Reduction of ground vibration by means of barriers or soil improvement along a railway track, Soil Dynamics and Earthquake Engineering 25 (2005) 701–716.

[8] Y. Yang, H. Hung, A parametric study of wave barriers for reduction of train-induced vibrations, International Journal for Numerical Methods in Engineering 40 (20) (1997) 3729–3747.

[9] X. Sheng, C. Jones, D. Thompson, Modelling ground vibrations from railways using wavenumber finite- and boundary-element methods, Proceedings of the Royal Society A - Mathematical, Physical and Engineering Sciences 461 (2005) 2043–2070.

[10] P. Coulier, S. François, G. Degrande, G. Lombaert, Subgrade stiffening next to the track as a wave impeding barrier for railway induced vibrations, Soil Dynamics and Earthquake Engineering 48 (2013) 119–131.

[11] http://www.rivas-project.eu (2011).

[12] P. Coulier, A. Dijckmans, S. François, G. Degrande, G. Lombaert, A spatial windowing technique to account for finite dimensions in 2.5D dynamic soil–structure interaction problems, Soil Dynamics and Earthquake Engineering 59 (2014) 51–67.

[13] L. Cremer, M. Heckl, B. Petersson, Structure-borne sound: Structural vibrations and sound radiation at audio frequencies, 3rd Edition, Springer, Berlin, 2005.

[14] B. Das, G. Ramana, Principles of soil dynamics, Cengage Learning, 2011.

[15] M. Ahearne, Y. Yang, A. El Haj, K. Then, K. Liu, Characterizing the viscoelastic properties of thin hydrogel-based constructs for tissue engineering applications, Journal of the Royal Society Interface 2 (5) (2005) 455–463.

[16] Y. Cao, D. Yang, W. Soboyejoy, Nanoindentation method for determining the initial contact and adhesion characteristics of soft polydimethylsiloxane, Journal of Materials Research 20 (8) (2005) 2004–2011.

[17] K. Liu, M. VanLandingham, T. Ovaert, Mechanical characterization of soft viscoelastic gels via indentation and optimization-based inverse finite element analysis, Journal of the Mechanical Behavior of Biomedical Materials 2 (4) (2009) 355–363.

[18] The MathWorks, MATLAB Image Processing Toolbox User's Guide (2013).